ACS APPLIED MATERIALS & INTERFACES

Research Article

www.acsami.org

Abnormal Excess Capacity of Conjugated Dicarboxylates in Lithium-Ion Batteries

Hyun Ho Lee,[†] Yuwon Park,[†] Kyoung-Hee Shin,[‡] Kyu Tae Lee,*[,†] and Sung You Hong*[,†]

[†]School of Energy and Chemical Engineering, KIER-UNIST Advanced Center for Energy, Ulsan National Institute of Science and Technology (UNIST), UNIST-gil 50, Ulsan 689-798, Republic of Korea

[‡]Korea Institute of Energy Research (KIER), 152 Gajeong-ro, Yuseong-gu, Daejeon 305-343, Republic of Korea

Supporting Information

ABSTRACT: Lithium-ion batteries (LIBs) are considered to be key energy storage systems needed to secure reliable, sustainable, and clean energy sources. Redox-active organic compounds have been proposed as interesting candidates for electrode materials for the next-generation LIBs because of their flexible molecular design, recyclability, and low production cost. Despite wide interest, a molecular-level understanding of the electrochemical lithiations/delithiations of those materials remains rudimentary. We synthesized a set of π-conjugated dicarboxylates and discovered unprecedented excess capacities for inverse-Wurster-type nonfused aromatic compounds (dilithium terephthalate and dilithium thiophene-2,5-dicarboxylate). Molecular structural investigations based on solid-state CP/MAS ^{13}C NMR combined with the stable isotope labeling method and ex situ X-ray diffraction were carried out to elucidate the origin of the excess reversible capacity. Interestingly, an open-chain-type dilithium muconate did not show an analogous behavior, signifying the key role played by the cyclic moiety in the electrochemical reaction.

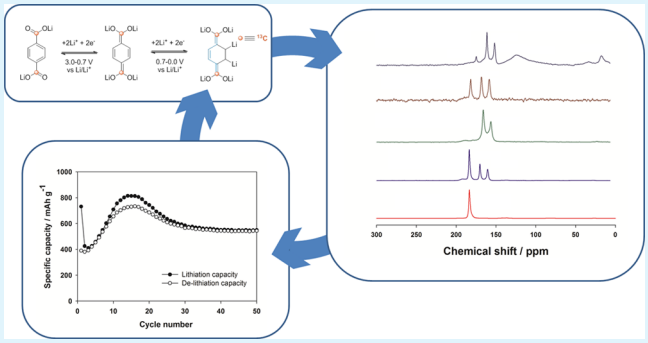

KEYWORDS: *lithium-ion batteries, organic electrode materials, anodes, excess capacity*

1. INTRODUCTION

Modern society has been depending heavily on nonrenewable fossil fuels, which have caused various kinds of damage to the environment including ocean acidification, climate change, and air pollution. In addition, the rising fuel prices and insecure petroleum imports act as global economic burdens. Some options for securing reliable, sustainable, and clean energy sources include harnessing the energy of solar radiation and wind. However, the electrical energy derived from solar radiation and wind needs to be stored, and lithium-ion batteries (LIBs) are considered to be key energy storage systems for this purpose.[1,2]

The design and synthesis of electrode materials for conventional LIBs have been mostly based on inorganic compounds, for example, $LiMO_2$, LiM_2O_4, and $LiMPO_4$ (M = Co, Ni, Fe, Mn, etc.) for use as cathode materials and silicon, silicon composites, graphite, and graphene for use as anode materials. Although the inorganic materials are proven to have excellent physical properties such as structural stability, redox potential, specific capacity, and electrical conductivity and typically exhibit high electrochemical performance, their structural modifications are not trivial, and in many cases, they are prepared through energy-intensive ceramic processes.

On the other hand, the organic electrode materials are typically prepared through low-cost solution phase routes. Flexible molecular design allows the exploration of diverse redox-active molecules exhibiting unique electrochemical properties.[3,4] Moreover, they are potentially recyclable and can be produced from biomass or natural compounds. For example, dilithium rhodizonate ($Li_2C_6O_6$) derived from D-glucose or *myo*-inositol has been applied to LIBs.[5] Recently, Lee et al. reformed proton-coupled electron-transfer reactions of flavin cofactors in mitochondria into lithium insertion/deinsertion reactions in LIBs via a biomimetic approach.[6] Properly designed flavin derivatives showed an improvement in the electrochemical performance metrics including redox potential, specific capacity, and cyclability.

The first application of an organic electrode material in a battery system was proposed by Williams et al. in 1969.[7] The lithium−dichloroisocyanuric acid couple was constructed for a primary battery. While redox-active conducting polymers including poly(acetylene), poly(aniline), and poly(pyrrole) have been evaluated for use in the lithium-ion rechargeable batteries,[8] the practical utilization of these materials has been hampered by their low thermal stability, low crystallinity, and solubility in polar organic electrolytes. In 2009, Tarascon and co-workers reported a seminal work on conjugated dicarboxylate anodes for LIBs.[9] Dilithium terephthalate (Li_2TP) salt was

Received: July 31, 2014
Accepted: October 6, 2014
Published: October 6, 2014

obtained through a simple acid−base reaction between terephthalic acid and lithium hydroxide, forming a monoclinic $P2_1/c$ crystal via ionic interactions of carboxylate groups with lithium cations and π-stacking interactions between planar terephthalates.[10] Li_2TP electrodes showed an outstanding electrochemical performance with stable cyclability, appropriate potential range, and enhanced thermal stability.

Conjugated organic compounds with ketone, carboxylate, anhydride, or imide functional groups have been demonstrated for LIBs[11−18] as well as sodium-ion batteries.[19−22] Recently, Chen et al. suggested molecular-level design strategies for organic electrode materials. Careful incorporation of heterocyclic aromatics or prearomatic 1,2-dicarbonyl moieties into the extended conjugated systems allowed the tunable redox potential, specific capacity, and rate capability needed for obtaining high-performance LIBs.[23,24]

According to Hünig's classification of multistage organic redox systems depicted in Scheme 1a, the reversible redox reaction of a π-conjugated dicarboxylate, which goes through a two-stage electron-transfer process with a radical-anion intermediate, belongs to system B.[25] Redox-active aromatic molecules are further categorized into Wurster and inverse-Wurster types (the end groups are located outside a cyclic π system and the aromaticity is found in either the reduced or oxidized form). Li_2TP fits into the inverse-Wurster type/system B category and is electrochemically reduced to a conjugated enolate tetralithium salt with two lithium insertions in the potential range of 3.0−0.7 V vs Li/Li^+.[9]

Scheme 1. (a) General Structures of Redox-Active Organic Molecules, Adapted from Hünig's Classification and (b) a Set of Synthesized Conjugated Dicarboxylates for Excess Capacity Studies

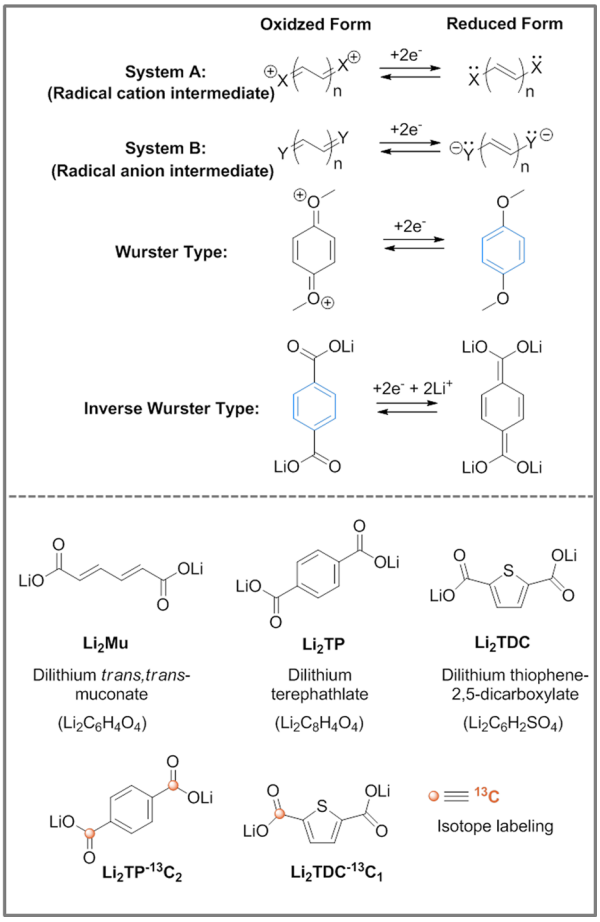

Herein, we report unprecedented excess capacities of nonfused aromatic compounds at low potential values below 0.7 V vs Li/Li^+. In order to conduct systematic comparative studies, we synthesized a family of π-conjugated dicarboxylates bearing linear and carbocyclic/heterocyclic aromatic moieties, as explained in Scheme 1b. The electrochemical lithiations/delithiations dependent on molecular structures were examined in these systems. Additionally, the charge/discharge mechanism will be discussed with the help of solid-phase ^{13}C NMR measurements, combined with stable isotope labeling and ex situ X-ray diffraction (XRD) analysis, to illustrate the molecular crystal transformations.

2. EXPERIMENTAL SECTION

General Information. Proton (^1H), carbon (^{13}C), and solid-state cross-polarization magic-angle-spinning (CP/MAS) ^{13}C NMR spectra were recorded on a Varian 600 spectrometer. Chemical shifts are given on the δ scale in parts per million, and coupling constants are in hertz. Solid-state CP/MAS ^{13}C NMR was performed at a spinning rate of 35 kHz with a 1.6 mm Agilent FastMAS probe. Electrochemical cells were dissembled, and the collected powder was filled into a probe in an argon-filled glovebox. Thermal analysis was performed at a heating rate of 10 °C min^{-1} under a nitrogen atmosphere using a TA Instrument Q600 thermogravimetric analyzer. Powder XRD data were collected on a Rigaku D/MAX2500 V/PC powder diffractometer using Cu Kα radiation (λ = 1.5405 Å) from 2θ = 15 to 35°. The specimens for ex situ XRD were prepared in an argon-filled glovebox. Coin cells were disassembled, and active materials were covered with beryllium windows. Scanning electron microscopy (SEM) samples were examined in a Nano 230 field-emission SEM instrument. Solvents and reagents were supplied from standard suppliers. Thin-layer chromatography was carried out on Merck Kieselgel 60 F254 silica-precoated glass plates. Plates were visualized using a UV lamp (λ_{max} = 254 nm) and/or developed with a potassium permanganate (0.5 g) in sodium hydroxide (1 M, 100 mL) solution.

Dilithium Terephthalate (Li_2TP). The title compound was prepared according to the previously described method.[9] Terephthalic acid (10.0 g, 60.2 mmol) was deprotonated by using $LiOH·H_2O$ (5.3 g, 126.3 mmol) in ethanol (200 mL). The mixture was stirred at room temperature for 24 h. A white solid was filtered and washed with ethanol several times. The powder was annealed at 150 °C for 9 h in vacuo. Yield: 10.5 g (97%). ^1H NMR (600 MHz, D_2O): δ_H 7.86 (s, 4H, Ar−C*H* × 4). ^{13}C NMR (150 MHz, D_2O): δ_C 175.2 (*C*═O), 138.5, 128.5 (Ar−*C*, Ar−*C*H). IR (ATR): 1567, 1388 cm^{-1}.

Dilithium Terephthalate-2,2′-$^{13}C_2$ (Li_2TP-$^{13}C_2$). Terephthalic acid-2,2′-$^{13}C_2$ (524 mg, 3.12 mmol; Sigma-Aldrich, 99% ^{13}C) was deprotonated by using $LiOH·H_2O$ (300 mg, 7.15 mmol) in ethanol (30 mL). The mixture was stirred at room temperature for 24 h. A white solid was filtered and washed with ethanol several times. The powder was annealed at 150 °C for 9 h in vacuo. Yield: 497 mg (88%). ^1H NMR (600 MHz, D_2O): δ_H 7.86 (s, 4H, Ar−C*H* × 4).

Dilithium *trans,trans*-Muconate (Li_2Mu).[9] *trans,trans*-Muconic acid (500 mg, 3.51 mmol) was deprotonated by $LiOH·H_2O$ (324 mg, 7.73 mmol) in ethanol (30 mL). The mixture was stirred at room temperature for 22 h. A white solid was filtered and washed with ethanol several times. The powder was annealed at 150 °C for 9 h in vacuo. Yield: 490 mg (91%). ^1H NMR (600 MHz, D_2O): δ_H 7.06−7.02 (m, 2H, vinyl C*H* × 2), 6.21−6.17 (m, 2H, vinyl C*H* × 2). ^{13}C NMR (151 MHz, D_2O): δ_C 175.1 (*C*═O), 138.5, 132.4 (vinyl CH). IR (ATR): 1617, 1552, 1382 cm^{-1}.

Dilithium Thiophene-2,5-dicarboxylate (Li_2TDC). Thiophene-2,5-dicarboxylic acid (2.00 g, 11.62 mmol) was deprotonated by $LiOH·H_2O$ (1.02 g, 24.39 mmol) in water (20 mL). The solution mixture was heated at 90 °C for 5 h. The reaction mixture was then recrystallized by the addition of ethanol and acetone to provide a white

dx.doi.org/10.1021/am505090p | ACS Appl. Mater. Interfaces 2014, 6, 19118−19126

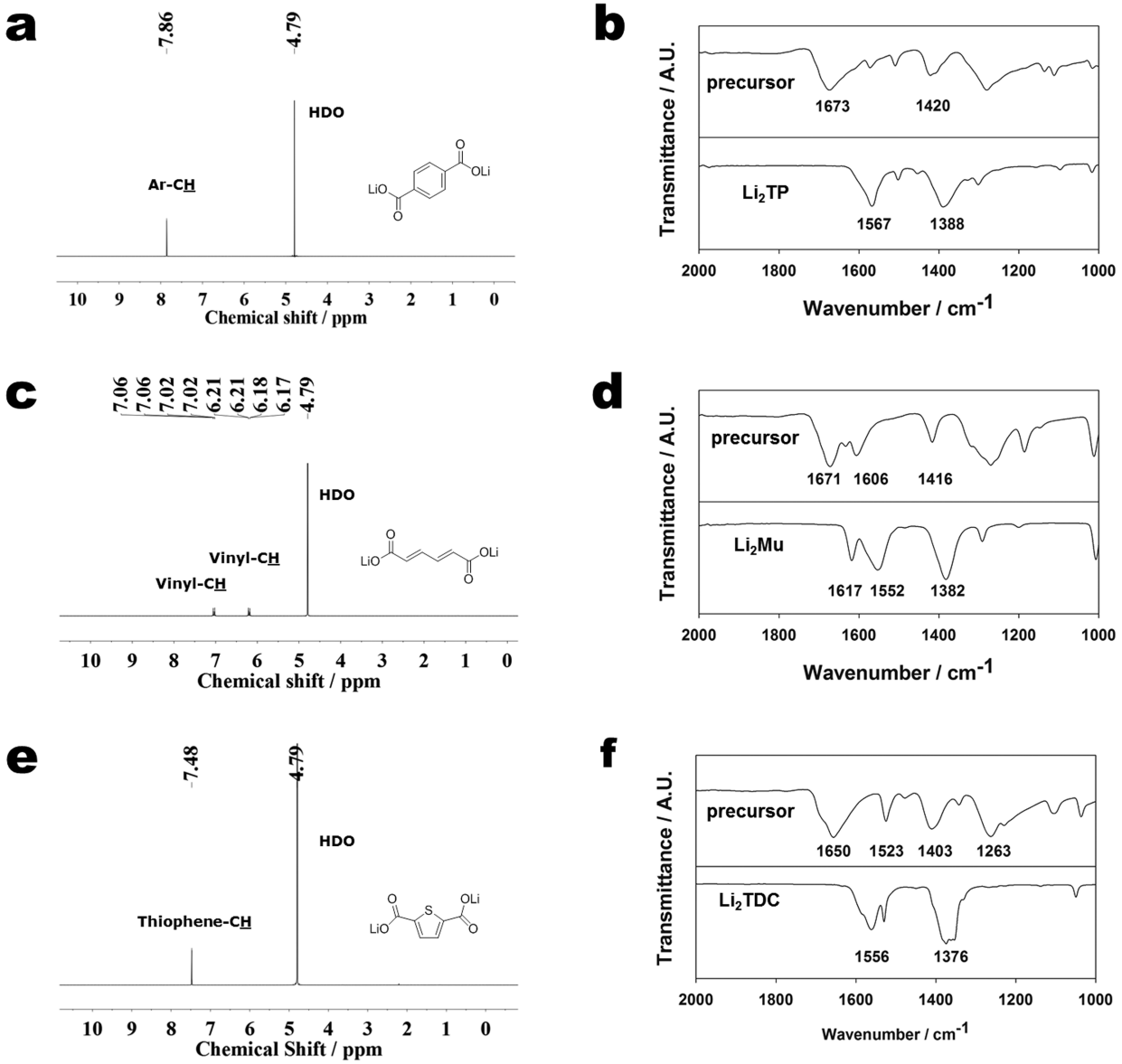

Figure 1. Spectroscopic characterization of a set of π-conjugated dicarboxylates. (a and b) ^{1}H NMR (600 MHz, D_2O) and IR spectra of Li_2TP. (c and d) ^{1}H NMR (600 MHz, D_2O) and IR spectra of Li_2Mu. (e and f) ^{1}H NMR (600 MHz, D_2O) and IR spectra of Li_2TDC.

precipitate. The powder was annealed at 150 °C for 8 h in vacuo. Yield: 1.58 g (74%). ^{1}H NMR (600 MHz, D_2O): δ_H 7.48 (s, 2H, thiophene C*H* × 2). ^{13}C NMR (151 MHz, D_2O): δ_C 169.6 (C═O), 144.4, 130.8 (thiophene *C*H). IR (ATR): 1556, 1376 cm $^{-1}$.

5-Ethyl-2-thiophenecarboxaldehyde-2-$^{13}C_1$ (5). To a solution of carbonyl-^{13}C-labeled *N*,*N*-dimethylformamide (DMF-^{13}C; 2.0 g, 27.0 mmol; carbonyl-^{13}C, 99%, Cambridge Isotope Laboratories, Inc.) in dichloromethane (DCM; 5 mL) was added $POCl_3$ (4.81 g, 31.4 mmol) slowly at 0 °C. After stirring for 2 h, a solution of 2-ethylthiophene (2.75 g, 24.5 mmol) in DCM (5 mL) was added dropwise over 40 min. The reaction mixture was then heated at 120 °C for 1.5 h and neutralized with $NaHCO_3$ (8.0 g) and cold water (150 mL). After extractions with DCM (150 mL × 3) and diethyl ether (150 mL × 3), the combined organic layer was dried over Na_2SO_4, filtered, and concentrated in vacuo. Flash column chromatography (*n*-hexane/ethyl acetate = 5/1) afforded the title compound as a yellow oil. Yield: 2.09 g (60%). ^{1}H NMR (600 MHz, $CDCl_3$): δ_H 9.82 (d, 1H, $^1J_{C-H}$ = 176.6 Hz, ^{13}C(═O)*H*), 7.61 (t, 1H, *J* = 3.8 Hz, thiophene C*H*), 6.92 (d, 1H, thiophene C*H*′), 2.92 (q, 2H, *J* = 7.5 Hz, CH_2), 1.35 (t, 3H, CH_3).

5-Formyl-2-thiophenecarboxylic Acid-2-$^{13}C_1$ (6). A suspension of potassium permanganate (2.01 g, 12.74 mmol) in acetone/water (20 mL, 1:1) was added to a solution of compound **5** (300 mg, 2.12 mmol) in acetone (10 mL) over 30 min. The solution was stirred and heated at 65 °C for 19 h. After concentration in vacuo, $Na_2S_2O_5$ (2.3 g) in 1 M HCl (70 mL) was added to give a precipitate. The white precipitate was filtered off, washed with 1 M HCl, and then dried in vacuo. Yield: 169 mg (47%). ^{1}H NMR (600 MHz, DMSO-d_6): δ_H 13.65 (brs, 1H, ^{13}COOH), 7.92 (d, 1H, *J* = 3.9 Hz, thiophene C*H*), 7.76−7.75 (m, 1H, thiophene C*H*′), 2.58 (s, 3H, CH_3).

Thiophene-2,5-carboxylic Acid-2-$^{13}C_1$ (7). To a suspension of compound **6** (527 mg, 3.08 mmol) in deionized water (20 mL) was added a NaOCl solution (4%, 17 mL). The mixture was stirred at 55 °C for 30 min. After filtration, an aqueous HCl solution (35%) was added. The white precipitate was filtered off, washed with 1 M HCl, and then dried in vacuo. Yield: 302 mg (57%). ^{1}H NMR (600 MHz, DMSO-d_6): δ_H 13.57 (brs, 2H, ^{13}COOH, COOH), 7.70−7.69 (m, 2H, thiophene C*H*, thiophene C*H*′).

Dilithium Thiophene-2,5-dicarboxylate-2-$^{13}C_1$ (Li_2TDC-$^{13}C_1$). Compound 7 (456 mg, 2.63 mmol) was deprotonated by LiOH·H_2O (262 mg, 6.24 mmol) in deionized water (25 mL). The solution

dx.doi.org/10.1021/am505090p | *ACS Appl. Mater. Interfaces* 2014, 6, 19118−19126

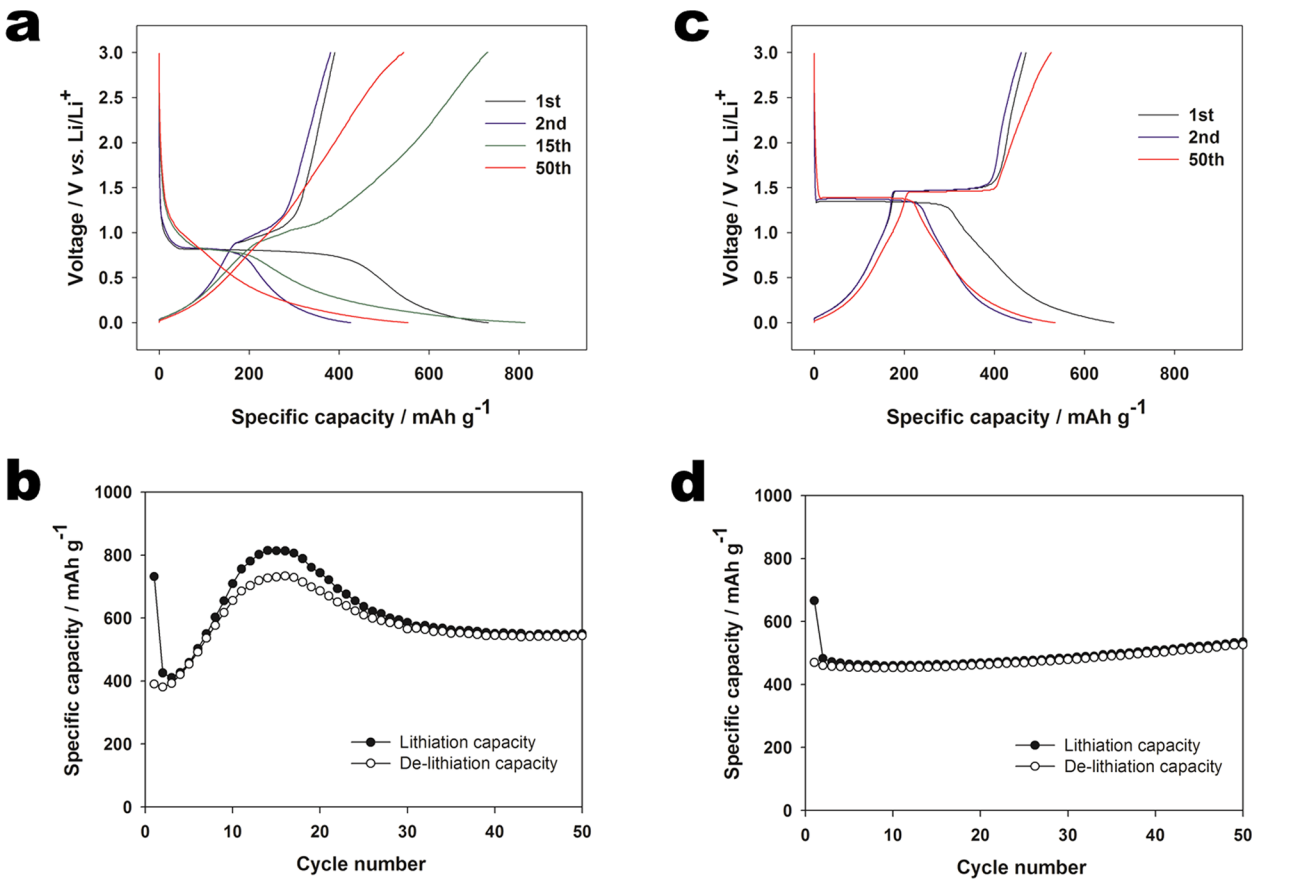

Figure 2. Electrochemical performances of Li_2TP and Li_2Mu electrodes. (a and b) Voltage profile and cyclability of Li_2TP. (c and d) Voltage profile and cyclability of Li_2Mu.

mixture was heated at 90 °C for 15 h. The reaction mixture was then recrystallized by the addition of ethanol and acetone to provide a white precipitate. The powder was annealed at 150 °C for 9 h in vacuo. Yield: 331 mg (68%). ^{1}H NMR (600 MHz, D_2O): δ_H 7.50 (m, 2H, thiophene C*H*, thiophene C*H*′). ^{13}C NMR (151 MHz, D_2O): δ_C 169.6 (^{13}COOH), 144.4 (m, thiophene *C*H), 130.8 (d, J = 4.0 Hz, thiophene *C*′H).

Electrochemical Characterization. The samples of electrochemically active materials were mixed with carbon black (Super P) and (carboxymethyl)cellulose in a 4:3:1 weight ratio. The electrochemical performance was evaluated using 2032 coin cells with a lithium metal anode and 0.8 M $LiPF_6$ in an ethylene carbonate and diethyl carbonate (1:1, v/v) electrolyte solution. Galvanostatic experiments were performed at a current density of 30 mA g^{-1} at 20 °C. Cyclic voltammetry (CV) was performed using a WonATech WBCS3000 instrument with a scanning rate of 20 μV s^{-1} in the voltage range of 0.0−3.0 V vs Li/Li$^+$. Via the van der Pauw method,[26] electronic conductivities of Li_2TP−Super P composites were measured.

3. RESULTS AND DISCUSSION

In order to clarify the effect of the molecular structure on electrochemical lithiation, the inverse-Wurster-type dilithium terephthalate (Li_2TP or $Li_2C_8H_4O_4$) and dilithium thiophene-2,5-dicarboxylate (Li_2TDC or $Li_2C_6H_2SO_4$) and the open-chain-type dilithium *trans,trans*-muconate (Li_2Mu or $Li_2C_6H_4O_4$) were prepared in acid−base chemistry (Scheme 1b).

As shown in Figure 1a, Li_2TP formation was confirmed with a single peak at 7.86 ppm in the ^{1}H NMR spectrum, which was assigned to the aromatic proton. The Fourier transform infrared (FT-IR) spectra showed asymmetric (ν_{as}) and symmetric (ν_s) carboxylate peaks at 1567 and 1388 cm^{-1}, respectively (Figure 1b). Thermogravimetric (TG) and differential thermal (DT) analyses were performed to verify the thermal stability and hydration status. Anhydrous Li_2TP decomposed above 575 °C, which provided evidence of its robust thermal stability (Figure S1 in the Supporting Information, SI). The XRD peaks also revealed that Li_2TP crystallized in a monoclinic cell with a space group of $P2_1/c$.[10]

The formation of Li_2Mu and Li_2TDC was confirmed by ^{1}H and ^{13}C NMR spectra (Figures 1c,e and S2 and S3 in the SI), by assigning vinyl or thiophene moieties with dicarboxylates. The FT-IR spectra clearly revealed removal of the dicarboxylic acid precursors after lithium hydroxide treatments and formation of the corresponding dilithium π systems (Figure 1d,f). According to TG/DT analyses, both Li_2Mu and Li_2TDC were anhydrous and showed high thermal stabilities with decomposition temperatures above 415 and 605 °C, respectively. As shown in the SEM images, the molecular crystals had various sizes and morphologies, mostly in the micrometer range (Figures S1−S3 in the SI).

The electrochemical investigations of Li_2TP ($Li_2C_8H_4O_4$) and Li_2Mu ($Li_2C_6H_4O_4$) were performed by galvanostatic charge/discharge in a half-cell using lithium foil as the counter electrode. Figure 2a shows the voltage profiles of the $Li_{2+x}C_8H_4O_4$/Li cell at a current density of 30 mA g^{-1} in the range of 0−3.0 V. The voltage profile of Li_2TP reveals a plateau located at about 0.81 V vs Li/Li$^+$ and a sloping region between 0.8 and 0 V. The plateau at 0.81 V is ascribed to enolization of the carboxylate (two lithium redox reactions), as demonstrated

dx.doi.org/10.1021/am505090p | ACS Appl. Mater. Interfaces 2014, 6, 19118−19126

Scheme 2. Proposed Excessive Lithiation Processes of Li_2Mu and Li_2TP

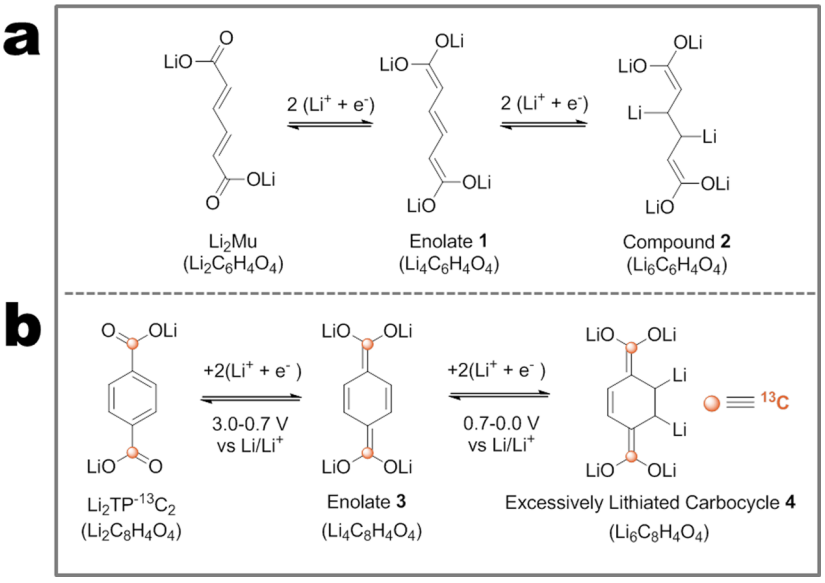

by Tarascon and co-workers.[9] A cyclic voltammogram of Li_2TP indicates clear cathodic and anodic peaks at 0.77 and 1.01 V vs Li/Li^+ (Figure S4 in the SI), which is consistent with the lithiation/delithiation profiles. The sloping region is indicative of lithium insertion into carbon (Super P), which delivers a reversible capacity of about 390 mAh g^{-1} (Figure S5 in the SI). Interestingly, a gradual capacity increase was observed for $Li_{2+x}C_8H_4O_4$ with a maximum discharge capacity of 815 mAh g^{-1} until 15 cycles, as shown in Figure 2b. However, the capacity gradually decreased to a value of 549 mAh g^{-1} after 50 cycles. Because of the insulating property of Li_2TP (Table S1 in the SI), the electrodes were prepared with a large amount of conductive carbon (Super P, 37.5%) to enhance the electrical conductivity of Li_2TP. Therefore, by subtraction of the capacity delivered from Super P (maximum 293 mAh g^{-1} = 390 mAh g^{-1} × 37.5 wt % Super P/50 wt % Li_2TP), the actual specific capacity of Li_2TP is found to be 522 mAh g^{-1} (equivalent to 3.5 lithium insertions) after 15 cycles. This surpasses the theoretical capacity (302 mAh g^{-1}) of Li_2TP calculated based on the two-lithium-insertion model (Scheme 1a). Additionally, the electrochemical performance of Li_2TP electrode was evaluated by galvanostatic charge/discharge in a half-cell at various current densities. When a current density is slowed down to 10 mA g^{-1} (Figure S6 in the SI), the maximum discharge capacity appears earlier at the ninth cycle with an increased value (discharge: 1072 mAh g^{-1}). It is noteworthy that an additional capacity of 264 mAh g^{-1} is observed at the maximum capacity point corresponding to an additional 1.75 lithium insertions. On the other hand, discharge/charge cycles at an increased current density (300 mA g^{-1}) do not reveal the maximum capacity point as well as the excess capacity of up to 40 cycles indicating that the abnormal excess capacity is affected by kinetics (current density).

In contrast, the excess capacity and capacity fading were not observed for linear Li_2Mu (Figure 2c,d), illustrating the key role played by the cyclic structure in the excessive lithiation process. During the initial cycles, a plateau corresponding to enolization of the carboxylate was observed at about 1.35 V with a narrow polarization gap of 90 mV. The actual reversible discharge capacity of Li_2Mu was 241 mAh g^{-1} after 50 cycles, which corresponds to 1.4 lithium insertions. Li_2Mu showed a capacity retention with a Coulombic efficiency of 99% after 50 cycles. As depicted in Scheme 2, two additional lithium insertions into enolate **1** destroy a conjugated triene moiety with the loss of the extra stabilization of the conjugated system. In addition, the degree of planarization of the linear π system will be reduced over the excessive lithiation process. The extended delocalization through the aligned neighboring π orbitals generates intramolecular planarization, which, in turn, stabilizes the π-extended conjugation systems during the electrochemical processes.[27] Excessive lithiation of linear (open-chain-type) Li_2Mu would be a thermodynamically unfavorable process because of the loss of the extended triene structure and the disturbed intramolecular planarity.[25] On the other hand, Li_2TP contains a rigid aromatic core, allowing facile copolarization in the solid state, and it can hold a conjugated triene moiety even after 4 lithium insertions. Therefore, Li_2TP, which is an inverse-Wurster-type redox system, has molecular structural benefits over the open-chain-type Li_2Mu.

In order to clarify the reaction mechanism for the excess capacity of the cyclic compound, ex situ solid-state CP/MAS ^{13}C NMR of $Li_{2+x}C_8H_4O_4$ was performed, and the results are shown in Figure 3. Although solution NMR typically allows a higher intrinsic sensitivity, a solid-state NMR analysis was chosen to better reflect the molecular crystal transformations in the solid-state carbon paste electrode. Besides, the artifacts associated with the solution-phase NMR measurements can also be circumvented. For example, a lithiated organic compound (organolithium) possesses highly polar C−Li bonds because of the significant electronegativity differences between carbon and lithium, which may cause side reactions with the NMR solvents. The low sensitivity of the solid-state ^{13}C NMR (Figure S7 in the SI) was enhanced by utilizing the stable isotope-labeling method, where ^{13}C-labeled dilithium terephthalate (Li_2TP-$^{13}C_2$) was designed and synthesized.

As shown in Figure 3, a pristine Li_2TP-$^{13}C_2$ sample exhibited a resonance line at 183.5 ppm, which was assigned to two equivalent carboxylate carbons. When the $Li_{2+x}C_8H_4O_4$/Li cell was initially discharged to 0.7 V, there were two new resonance lines at 170.2 and 160.9 ppm, which were assigned to enolate **3**

dx.doi.org/10.1021/am505090p | ACS Appl. Mater. Interfaces 2014, 6, 19118−19126

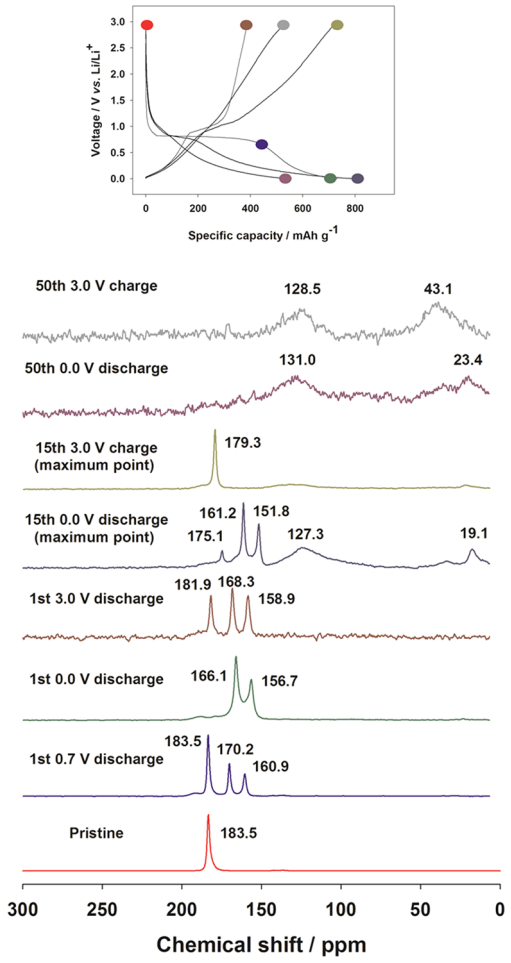

Figure 3. Solid-State CP/MAS ^{13}C NMR analysis of the Li_2TP-$^{13}C_2$ electrode.

via two lithium insertions (Scheme 2b). The two new lines may arise because of the different intermolecular packing or isomeric (i.e., keto−enol tautomeric) states, which is analogous to the imine−enamine tautomerism, as suggested by the Choi and Coskun group.[15] Yet, two phases of pristine Li_2TP and **3** are observed together, indicating partial electrochemical reduction of Li_2TP. When Li_2TP was further lithiated to 0 V, the resonance lines from **3** became apparent. When Li_2TP was delithiated to 3.0 V, the Li_2TP-$^{13}C_2$ phase reemerged, illustrating the reversibility of electrochemical lithiation/delithiation. After 15 cycles, broad signals were observed primarily in the upfield (olefinic and aliphatic) region at about 137 ppm and close to 19 ppm, which were assigned to further reduced carbocycle **4** ($Li_6C_8H_4O_4$). This explains the excess capacity of the Li_2TP electrode. During the subsequent delithiation, the carboxylate signal (179.3 ppm) was fully recovered, indicating the reversible formation of Li_2TP. After 50 cycles, the characteristic resonance lines from Li_2TP-$^{13}C_2$ and **3** ($Li_4C_8H_4O_4$) were not detected anymore. The reduced specific capacity of the $Li_{2+x}C_8H_4O_4$/Li cell due to decomposition of the Li_2TP and intermediate **3** can cause capacity fading of the Li_2TP electrode, as shown in Figure 2b. To the best of our knowledge, the excess capacity of a nonfused aromatic compound and its confirmation through solid-state NMR analysis are unprecedented, although there are a few reports on the excess capacity of multifused aromatic rings including nanographene and 1,4,5,8-naphthalenetetracarboxylic dianhydride.[28,29]

Electrochemical lithiation of the Li_2TP electrode was further studied using ex situ powder XRD and SEM analyses. For clarity, the XRD patterns were recorded in the $2\theta_{Cu\ K\alpha}$ = 15−35° range. Pristine Li_2TP shows the main Bragg peaks near $2\theta_{Cu\ K\alpha}$ = 20.3°, 21.0°, 23.2°, 24.1°, and 29.8°, which were indexed to the (011), (110), (002), (111), (102), and (112) planes. During the initial discharge in the potential range of 3.0−0.7 V (Figure 4), new Bragg peaks near $2\theta_{Cu\ K\alpha}$ = 23.7°,

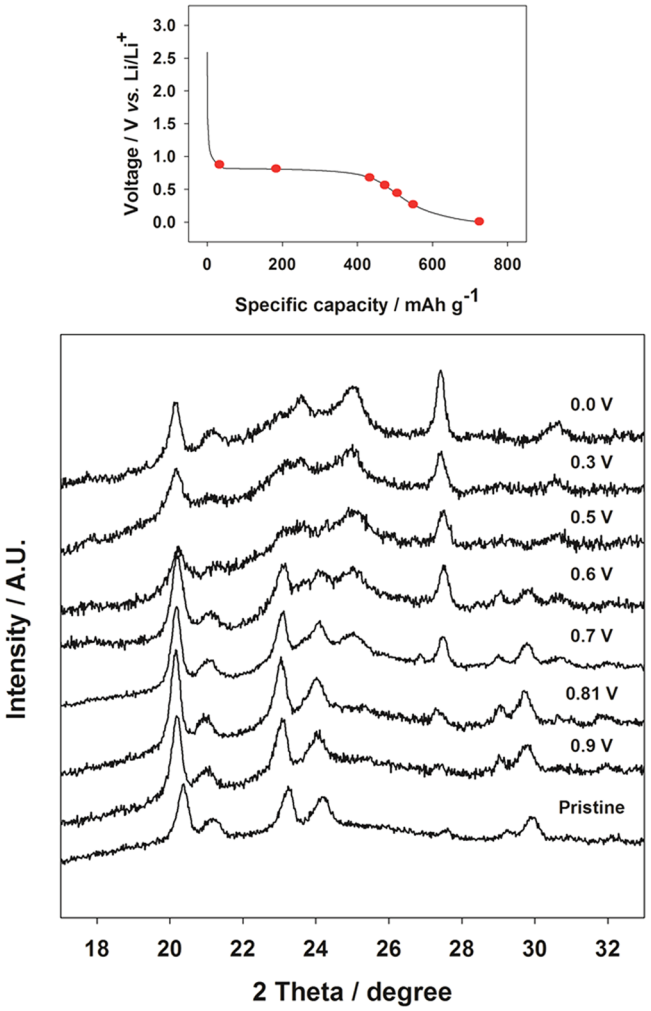

Figure 4. Ex situ powder XRD analysis of the Li_2TP electrode during the initial discharge.

25.2°, and 30.9° were observed, which corresponds to formation of the enolate **3** phase[9] along with the pristine Li_2TP phase. The two-phase (Li_2TP/enolate **3**) reaction was consistently found in previously mentioned voltage profiles [showing a distinctive plateau at 0.81 V vs Li/Li^+ (Figure 2a)] as well as the solid-state NMR analysis (Figure 3). From 0.6 to 0 V, the new XRD pattern of enolate **3** becomes apparent with a decrease in the intensity of the major Bragg peaks of Li_2TP, implying the gradual conversion of Li_2TP to enolate **3** ($Li_4C_8H_4O_4$). When the cell was charged (Figure 5), the major Bragg peaks of $Li_{2+x}C_8H_4O_4$ were superimposed on the pattern for pristine Li_2TP, indicating a fully reversible redox process. After the recharging from 0 to 3.0 V, the Bragg peaks corresponding to the two phases of Li_2TP and enolate **3** were

dx.doi.org/10.1021/am505090p | ACS Appl. Mater. Interfaces 2014, 6, 19118−19126

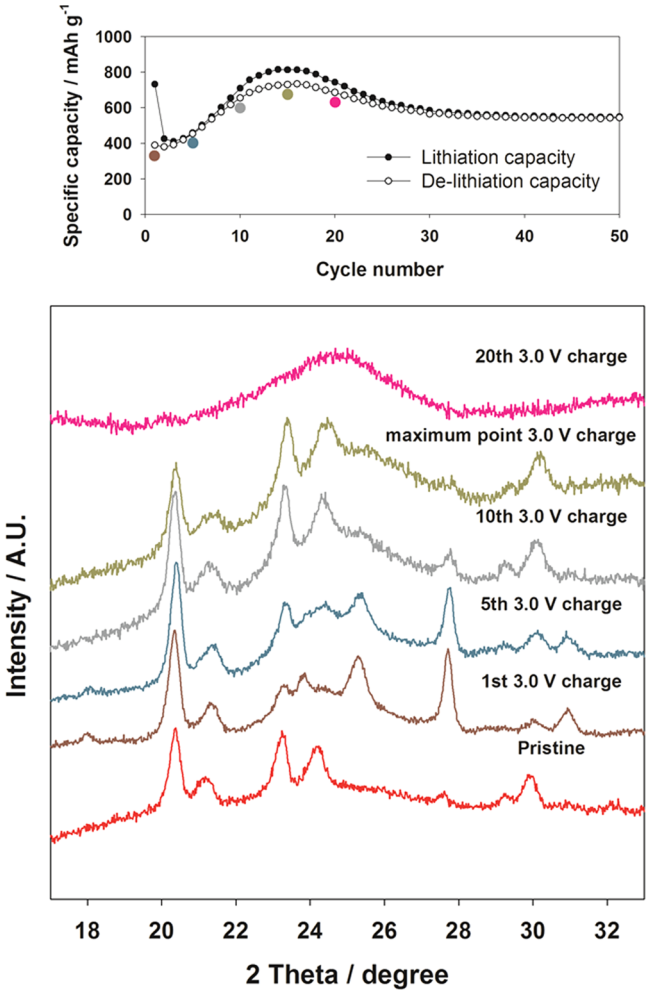

Figure 5. Ex situ powder XRD analysis of the Li_2TP electrode during charge/discharge cycles.

seen again. The Li_2TP phase became clearer and broader after 10 cycles. However, the XRD pattern of Li_2TP was not detected after 20 cycles, which is attributed to either amorphization of the molecular crystal or the gradual degradation of Li_2TP, as seen from the solid-state NMR analysis and voltage profiles. The morphological changes of the Li_2TP electrode were examined by SEM. The initial electrode paste contained microsized (ca. 1−2 μm) Li_2TP particles (see Figures S1c and S8 in the SI). After 10 cycles, however, the SEM image of the paste revealed different morphological features having coral-like structures with the disappearance of microcrystalline particles. The electrochemical lithiation process of the Li_2TP electrode can be more effectively carried out because of the shortened diffusion path of large crystalline Li_2TP particles after 10 cycles.

Li_2TDC, which is a heterocyclic dicarboxylate, was compared to Li_2TP to further support the effect of the cyclic structure on the excess capacity. The thiophene core was selected as a benzene analogue because it creates an aromatic 6π system (Scheme 1b). The 3p orbital of sulfur has poor overlap with the 2p orbital of carbon, hindering the π donation of the sulfur lone-pair electrons to the aromatic core.[30] Moreover, sulfur has electronegativity values similar to those of carbon (χ_p(S) = 2.58; χ_p(C) = 2.55; Pauling electronegativity). Therefore, Li_2TDC was expected to possess electrochemical properties similar to those of Li_2TP. The electrochemical performance of Li_2TDC was evaluated in a half-cell using a lithium foil as the counter electrode. Figure 6 shows the voltage profiles of

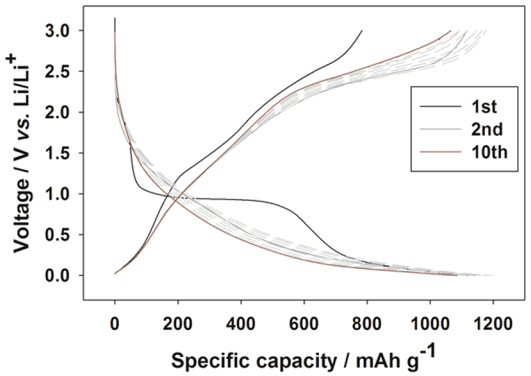

Figure 6. Voltage profile of the Li_2TDC electrode at 30 mA g^{-1} between 3.0 and 0 V.

Li_2TDC measured at a current density of 30 mA g^{-1}. Similar to the observations on Li_2TP, an exceptionally high discharge capacity of 1143 mAh g^{-1} associated with excess capacity was observed in the case of Li_2TDC. After removal of the Super P contribution, the actual capacity of Li_2TDC was calculated to be 850 mAh g^{-1}, which is equivalent to 5.8 lithium insertions. However, Li_2TDC did not require multiple cycles to reach the maximum capacity value, as observed for Li_2TP.

For the high-resolution solid-state CP/MAS ^{13}C NMR studies, ^{13}C-labeled dilithium thiophene-2,5-dicarboxylate (Li_2TDC-$^{13}C_1$) was designed and synthesized through formylation and oxidation followed by an acid−base reaction, as depicted in Scheme 3. A thiophene derivative **5** was obtained

Scheme 3. Synthesis of Li_2TDP-$^{13}C_1$[a]

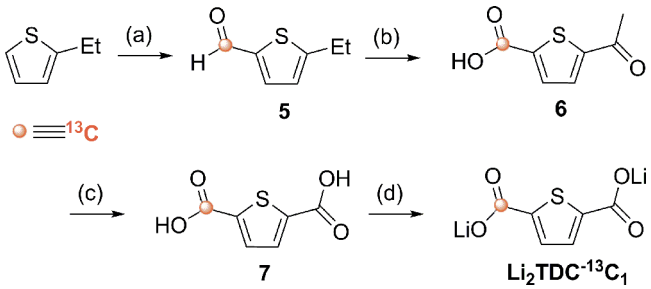

[a](a) $POCl_3$, DMF-^{13}C, DCM, 60%. (b) $KMnO_4$, acetone/H_2O, 47%. (c) NaOCl, H_2O, 57%. (d) LiOH, H_2O, 68%.

by the regioselective formylation of 2-ethylthiophene by using phosphoryl chloride and DMF-^{13}C under the Vilsmeier condition. The benzylic carbon was oxidized to ketone by potassium permanganate to afford **6**, and the intermediate was further oxidized to **7** using NaOCl. The dicarboxylic acid **7** was then finally deprotonated to furnish the corresponding lithium salt, Li_2TDC ($Li_2C_6H_2SO_4$)-$^{13}C_1$.

When the $Li_{2+x}C_6H_2SO_4$/Li cell was initially discharged to 0 V vs Li/Li^+, the solid-state CP/MAS ^{13}C NMR spectra (Figure 7) exhibited broad signals in the upfield region (δ_c of about 120−50 ppm falling to olefinic and aliphatic carbons), which are assigned to the excessively lithiated compound(s). Similar patterns were observed after the second discharge cycle. When the cell was recharged to 3.0 V, the carboxylate signal reappeared, indicating the reversible formation of Li_2TDC-$^{13}C_1$.

dx.doi.org/10.1021/am505090p | ACS Appl. Mater. Interfaces 2014, 6, 19118−19126

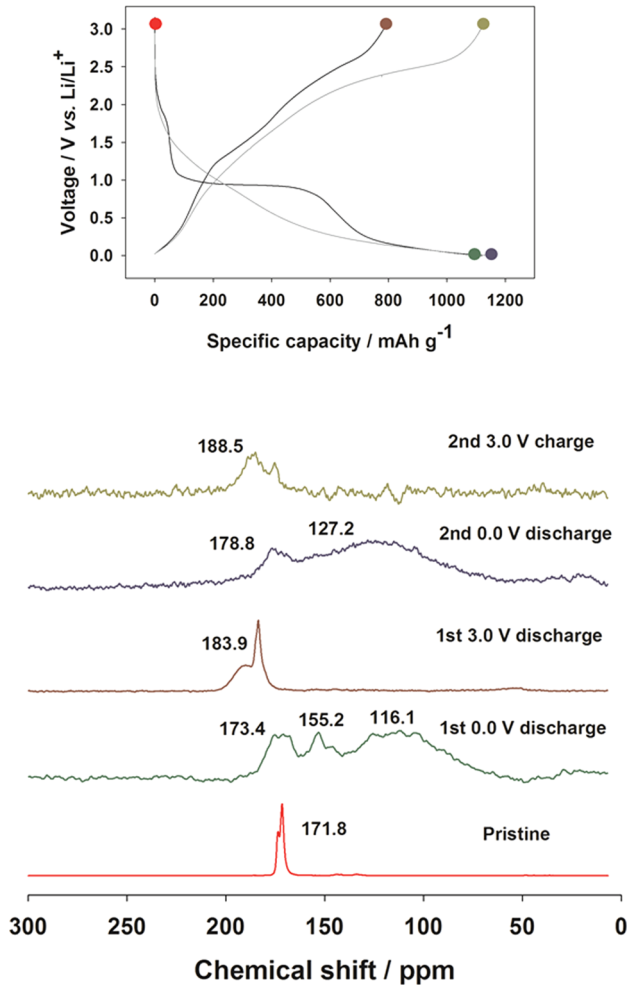

Figure 7. Solid-State CP/MAS ^{13}C NMR analysis of the Li_2TDC-$^{13}C_1$ electrode.

A chemical shift variation, closely associated with the orientation of the molecular crystals, was found for the carboxylate carbon of Li_2TDC-$^{13}C_1$ (171.8 ppm for the pristine sample and 188.5 ppm for the recharged sample). In order to confirm the crystallographic changes of the $Li_{2+x}C_6H_2SO_4$/Li cell, ex situ powder XRD measurements were performed, which showed progressive amorphization during the initial cycles (Figure S9 in the SI).

4. CONCLUSIONS

In summary, a series of π-conjugated (linear, carbocyclic, and heterocyclic) dicarboxylates were synthesized to determine the effect of the molecular structure on the excess capacity. The origin of the excess reversible capacity of nonfused aromatic compounds (Li_2TP and Li_2TDC) was studied through the voltage profiles, solid-state CP/MAS ^{13}C NMR measurements and ex situ powder XRD analysis. Synthesis of ^{13}C-isotope-labeled Li_2TP and Li_2TDC allowed the measurement of high-resolution solid-state NMR spectra, which exhibited characteristic chemical shifts assigned to excessive lithiation states in a low potential range below 0.7 V vs Li/Li^+. Ex situ powder XRD measurements further revealed molecular crystal transformations during electrochemical lithiations/delithiations. Unlike the excess capacities of the inverse-Wurster-type carbocyclic and heterocyclic aromatic compounds (Li_2TP and Li_2TDC, respectively), the open-chain-type π-conjugated Li_2Mu with a linear geometry did not show excessive lithiation, implying the key role played by the cyclic core on the excess capacity of conjugated systems. The data from these experiments suggest that systematic studies assisted by synthetic organic chemistry and solid-state analyses can be a pivotal step toward revealing the molecular-structure-dependent electrochemical performance of LIBs.

■ ASSOCIATED CONTENT

Ⓢ Supporting Information

^1H and/or ^{13}C NMR spectra of Li_2TP, Li_2Mu, Li_2TDC, compounds **5**–**7**, Li_2TP-$^{13}C_2$, and Li_2TDC-$^{13}C_1$, XRD patterns, SEM images, TG and DT analyses, CV and voltage profiles of Li_2TP, electrochemical performances of Super P, solid-state ^{13}C NMR of Li_2TP without ^{13}C isotope labeling, and additional figures including Figures S1–S14. This material is available free of charge via the Internet at http://pubs.acs.org.

■ AUTHOR INFORMATION

Corresponding Authors

*E-mail: ktlee@unist.ac.kr.
*E-mail: syhong@unist.ac.kr.

Author Contributions

The manuscript was written through contributions of all authors. All authors have given approval to the final version of the manuscript.

Notes

The authors declare no competing financial interest.

■ ACKNOWLEDGMENTS

This work was supported by the Korea Institute of Energy and Research (KIER) (B4-2424), the National Research Foundation of Korea (NRF-2013R1A1A2060695), the MSIP (Ministry of Science, ICT & Future Planning), Korea, under the C-ITRC (Convergence Information Technology Research Center) support program (NIPA-2013-H0301-13-1009) supervised by the NIPA (National IT Industry Promotion Agency), and by Korea Electrotechnology Research Institute (KERI) Primary research program through the National Research Council of Science & Technology funded by the Ministry of Science, ICT and Future Planning (MSIP) (No. 14-12-N0101-69). We are grateful to Jin Wook Kim for measuring the electrical conductivities of Li_2TP–Super P composites and Prof. Yoon Seok Jung for helpful discussions.

■ REFERENCES

(1) Goodenough, J. B.; Park, K.-S. The Li-Ion Rechargeable Battery: a Perspective. *J. Am. Chem. Soc.* **2013**, *135*, 1167–1176.
(2) Goodenough, J. B. Electrochemical Energy Storage in a Sustainable Modern Society. *Energy Environ. Sci.* **2014**, *7*, 14–18.
(3) Liang, Y.; Tao, Z.; Chen, J. Organic Electrode Materials for Rechargeable Lithium Batteries. *Adv. Energy Mater.* **2012**, *2*, 742–769.
(4) Poizot, P.; Dolhem, F. Clean Energy New Deal for a Sustainable World: from Non-CO_2 Generating Energy Sources to Greener Electrochemical Storage Devices. *Energy Environ. Sci.* **2011**, *4*, 2003–2019.
(5) Chen, H.; Armand, M.; Demailly, G.; Dolhem, F.; Poizot, P.; Tarascon, J.-M. From Biomass to a Renewable $Li_XC_6O_6$ Organic Electrode for Sustainable Li-Ion Batteries. *ChemSusChem* **2008**, *1*, 348–355.
(6) Lee, M.; Hong, J.; Seo, D. H.; Nam, D. H.; Nam, K. T.; Kang, K.; Park, C. B. Redox Cofactor from Biological Energy Transduction as Molecularly Tunable Energy-Storage Compound. *Angew. Chem., Int. Ed.* **2013**, *52*, 8322–8328.

(7) Williams, D. L.; Byrne, J. J.; Driscoll, J. S. A High Energy Density Lithium/Dichloroisocyanuric Acid Battery System. *J. Electrochem. Soc.* **1969**, *116*, 2−4.
(8) Novák, P.; Müller, K.; Santhanam, K. S. V.; Haas, O. Electrochemically Active Polymers for Rechargeable Batteries. *Chem. Rev.* **1997**, *97*, 207−282.
(9) Armand, M.; Grugeon, S.; Vezin, H.; Laruelle, S.; Ribiere, P.; Poizot, P.; Tarascon, J. M. Conjugated Dicarboxylate Anodes for Li-ion Batteries. *Nat. Mater.* **2009**, *8*, 120−125.
(10) Kaduk, J. Terephthalate Salts: Salts of Monopositive Cations. *Acta Crystallogr., Sect. B: Struct. Sci.* **2000**, *56*, 474−485.
(11) Chen, H.; Armand, M.; Courty, M.; Jiang, M.; Grey, C. P.; Dolhem, F.; Tarascon, J.-M.; Poizot, P. Lithium Salt of Tetrahydroxybenzoquinone: Toward the Development of a Sustainable Li-Ion Battery. *J. Am. Chem. Soc.* **2009**, *131*, 8984−8988.
(12) Gottis, S.; Barrès, A.-L.; Dolhem, F.; Poizot, P. Voltage Gain in Lithiated Enolate-Based Organic Cathode Materials by Isomeric Effect. *ACS Appl. Mater. Interfaces* **2014**, *6*, 10870−10876.
(13) Walker, W.; Grugeon, S.; Mentre, O.; Laruelle, S.; Tarascon, J.-M.; Wudl, F. Ethoxycarbonyl-Based Organic Electrode for Li-Batteries. *J. Am. Chem. Soc.* **2010**, *132*, 6517−6523.
(14) Wang, S.; Wang, L.; Zhang, K.; Zhu, Z.; Tao, Z.; Chen, J. Organic $Li_4C_8H_2O_6$ Nanosheets for Lithium-Ion Batteries. *Nano Lett.* **2013**, *13*, 4404−4409.
(15) Kim, D. J.; Je, S. H.; Sampath, S.; Choi, J. W.; Coskun, A. Effect of N-Substitution in Naphthalenediimides on the Electrochemical Performance of Organic Rechargeable Batteries. *RSC Adv.* **2012**, *2*, 7968−7970.
(16) Renault, S.; Brandell, D.; Gustafsson, T.; Edstrom, K. Improving the Electrochemical Performance of Organic Li-Ion Battery Electrodes. *Chem. Commun.* **2013**, *49*, 1945−1947.
(17) Aragón, M. J.; León, B.; Pérez Vicente, C.; Tirado, J. L.; Chadwick, A. V.; Berko, A.; Beh, S.-Y. Cobalt Oxalate Nanoribbons as Negative-Electrode Material for Lithium-Ion Batteries. *Chem. Mater.* **2009**, *21*, 1834−1840.
(18) Burkhardt, S. E.; Bois, J.; Tarascon, J.-M.; Hennig, R. G.; Abruña, H. D. Li-Carboxylate Anode Structure−Property Relationships from Molecular Modeling. *Chem. Mater.* **2012**, *25*, 132−141.
(19) Park, Y.; Shin, D. S.; Woo, S. H.; Choi, N. S.; Shin, K. H.; Oh, S. M.; Lee, K. T.; Hong, S. Y. Sodium Terephthalate as an Organic Anode Material for Sodium Ion Batteries. *Adv. Mater.* **2012**, *24*, 3562−3567.
(20) Zhao, L.; Zhao, J.; Hu, Y.-S.; Li, H.; Zhou, Z.; Armand, M.; Chen, L. Disodium Terephthalate ($Na_2C_8H_4O_4$) as High Performance Anode Material for Low-Cost Room-Temperature Sodium-Ion Battery. *Adv. Energy Mater.* **2012**, *2*, 962−965.
(21) Abouimrane, A.; Weng, W.; Eltayeb, H.; Cui, Y.; Niklas, J.; Poluektov, O.; Amine, K. Sodium Insertion in Carboxylate Based Materials and Their Application in 3.6 V Full Sodium Cells. *Energy Environ. Sci.* **2012**, *5*, 9632−9638.
(22) Chihara, K.; Chujo, N.; Kitajou, A.; Okada, S. Cathode Properties of $Na_2C_6O_6$ for Sodium-Ion Batteries. *Electrochim. Acta* **2013**, *110*, 240−246.
(23) Liang, Y.; Zhang, P.; Chen, J. Function-Oriented Design of Conjugated Carbonyl Compound Electrodes for High Energy Lithium Batteries. *Chem. Sci.* **2013**, *4*, 1330−1337.
(24) Liang, Y.; Zhang, P.; Yang, S.; Tao, Z.; Chen, J. Fused Heteroaromatic Organic Compounds for High-Power Electrodes of Rechargeable Lithium Batteries. *Adv. Energy Mater.* **2013**, *3*, 600−605.
(25) Deuchert, K.; Hünig, S. Multistage Organic Redox Systems—A General Structural Principle. *Angew. Chem., Int. Ed.* **1978**, *17*, 875−886.
(26) van der Paw, L. J. A Method of Measuring the Resistivity and Hall Coefficient on Lamellae of Arbitrary Shape. *Philips Technol. Rev.* **1958**, *20*, 220−224.
(27) Meerholz, K.; Gregorius, H.; Müllen, K.; Heinze, J. Voltammetric Studies of Solution and Solid-State Properties of Monodisperse Oligo(*p*-phenylenevinylene)s. *Adv. Mater.* **1994**, *6*, 671−674.
(28) Yang, S.; Feng, X.; Zhi, L.; Cao, Q.; Maier, J.; Müllen, K. Nanographene-Constructed Hollow Carbon Spheres and Their Favorable Electroactivity with Respect to Lithium Storage. *Adv. Mater.* **2010**, *22*, 838−842.
(29) Han, X.; Qing, G.; Sun, J.; Sun, T. How Many Lithium Ions Can Be Inserted Onto Fused C_6 Aromatic Ring Systems? *Angew. Chem., Int. Ed.* **2012**, *51*, 5147−5151.
(30) Fleming, I. *Molecular Orbitals and Organic Chemical Reactions*; John Wiley & Sons, Ltd.: New York, 2009.